X-RAY FLUORESCENCE/AUGER-ELECTRON COINCIDENCE SPECTROSCOPY OF VACANCY CASCADES IN ATOMIC ARGON

U. Arp[†], T. LeBrun[‡], S.H. Southworth[‡], M.A. MacDonald[¶], and M. Jung[‡]

[†]Electron and Optical Physics Division, National Institute of Standards and Technology, Gaithersburg, MD 20899, U.S.A.

[‡]Physics Division, Argonne National Laboratory, Argonne, IL 60439, U.S.A.

[¶]E.P.S.R.C. Daresbury Laboratory, Warrington WA4 4AD, United Kingdom

Date: 1 December 1996

PACS: 32.80.Hd, 32.50.+d, 31.20.Di

In preparation for: Phys. Rev. A

Abstract.

Argon $L_{2,3}$-$M_{2,3}M_{2,3}$ Auger-electron spectra were measured in coincidence with Kα fluorescent x-rays in studies of Ar K-shell vacancy decays at several photon energies above the K-threshold and on the 1s – 4p resonance in atomic argon. The complex spectra recorded by conventional electron spectroscopy are greatly simplified when recorded in coincidence with fluorescent x-rays, allowing a more detailed analysis of the vacancy cascade process. The resulting coincidence spectra are compared with Hartree-Fock calculations which include shake-up transitions in the resonant case. Small energy shifts of the coincident electron spectra are attributed to post-collision interaction with 1s photoelectrons.

1. Introduction

The photoexcitation/ionization of a deep inner-shell in a many-electron atom is followed by a multi-step vacancy cascade process in which vacancies are transferred to the outer shells[1 2 3 4 5 6 7 8 9 10 11 12 13]. The great variety of intermediate multi-vacancy configurations in this decay cascade causes very complex Auger-spectra, which are usually interpreted on the basis of spectator-hole satellite models[11 13]. The de-excitation process involves a highly correlated many-particle system, in which angular correlations between the emitted particles, multiple post-collision interactions (PCI) and interference between different decay pathways leading to the same final state can play important roles. In addition, close to thresholds or resonances, excitation and decay processes are coupled and must be treated using scattering approaches[14].

Busch and co-workers[11] presented argon electron spectra in the energy range of the L-MM Auger-transitions after broadband photoexcitation/ionization. The interpretation of their data was complicated by the multi-vacancy nature of the initial state after photon impact, since they created a mixture of atoms with holes in the K, L and M shells.

---

[1]T.A. Carlson and M.O. Krause, Phys. Rev. 137, A1655 (1965).
[2]J.C. Levin, C. Biedermann, N. Keller, L. Liljeby, C.-S. O, R.T. Short, I.A. Sellin, and D.W. Lindle, Phys. Rev. Lett. 65, 988 (1990).
[3] K. Ueda, E. Shigemasa, Y. Sato, A. Yagishita, M. Ukai, H. Maezawa, T. Hayaishi, and T. Sasaki, J. Phys. B: At. Mol. Opt. Phys. 24, 605 (1991).
[4]G. Omar and Y. Hahn, Phys. Rev. A 44, 483 (1991).
[5]J. Doppelfeld, N. Anders, B. Esser, F. von Busch, H. Scherer, and S. Zins, J. Phys. B: At. Mol. Opt. Phys. 26, 445 (1993).
[6]T. Hayaishi, E. Murakami, Y. Morioka, E. Shigemasa, A. Yagishita, and F. Koike, J. Phys. B: At. Mol. Opt. Phys. 27, L115 (1994).
[7]A.G. Kochur, V.L. Sukhorukov, A.I. Dudenko, and Ph.V. Demekhin, J. Phys. B: At. Mol. Opt. Phys. 28, 387 (1995).
[8]D.V. Morgan, R.J. Bartlett, and M. Sagurton, Phys. Rev. A 51, 2939 (1995).
[9]S.H. Southworth, M.A. MacDonald, T. LeBrun, Y. Azuma, and J.W. Cooper, in *Atomic Physics at High Brilliance Synchrotron Sources*, edited by H.G. Berry, P. Cowan, and D. Gemmell (Argonne, DOE, 1994), p. 205.
[10]S.H. Southworth, M.A. MacDonald, T. LeBrun, and Y. Azuma, in *16th Int. Conf. On X-Ray and Inner-Shell Processes X-93*, edited by L. Sarkadi and D. Berenyi (Debrecen, 1993).
[11]F. von Busch, J. Doppelfeld, C. Günther, and E. Hartmann, J. Phys. B: At. Mol. Opt. Phys. 27, 2151 (1994).
[12]H. Kjeldsen, T.D. Thomas, P. Lablanque, M. Lavollée, F. Penent, M. Hochlaf, and R.I. Hall, J. Phys. B: At. Mol. Opt. Phys. 29, 1689 (1996).
[13]A.G. Kochur and V.L. Sukhorukov, J. Elec. Spectr. Rel. Phenom. 76, 325 (1995).
[14]T. Åberg and B. Crasemann, in *Resonant Anomalous X-Ray Scattering: Theory and Applications*, edited by G. Materlik, C.J. Sparks, and K. Fischer (North-Holland, Amsterdam, 1994), p. 431.

Southworth *et al.*[9] [10] presented electron spectra in the same energy range after excitation with monochromatized x-rays which were, as well as the data of Busch *et al.*[11], later interpreted by Kochur and Sukhorukov[13] using a straight-forward single-configuration Hartree-Fock model to construct de-excitation trees.

Fig. 1 demonstrates the complexity of the argon cascade electron spectra in the energy region of the $L_{2,3}$-MM Auger-transitions after 1s photoionization/excitation. The spectra in fig. 1 were recorded with an exciting x-ray bandwidth of $\Delta\hbar\omega \approx 0.8$ eV and using a cylindrical mirror electron analyzer at medium resolution (bandwidth $\Delta E \approx 0.5$ eV) (same as reported in refs.[9] [10] [15]). The spectrum recorded 32.7 eV below the 1s threshold (1A) energy results from direct photoionization of the L subshells and is similar to earlier results measured at energies in the vicinity of the 2p thresholds[16] [17] [18] [19], except that electron-correlation satellites are strongly enhanced. Cooper *et al.*[20] showed that the satellites are enhanced due to $L_1 - L_{2,3}$ vacancy transfers via L_1-$L_{2,3}$ M Coster-Kronig decay of the L_1 vacancies produced by photoionization. When the x-ray energy is tuned to the 4p resonance (1C) or 4.9 eV above threshold (1B), $L_{2,3}$ vacancies are produced predominantly by K-LL and K-LM Auger-decays of the initial K-vacancies produced (see Kochur *et al.*[7] for details on calculated branching ratios). The resulting $L_{2,3}$-MM Auger-spectra are very complex due to overlapping or unresolved transitions from alternative decay pathways.

Despite the complexity of the spectra in Fig. 1, some general results can be derived. First, excitation of the 1s electron to the 4p resonance (1C) produces a vacancy cascade spectrum very different from that produced above the 1s ionization threshold (1B), i.e.,

---

[15] S.H. Southworth, M.A. MacDonald, T. LeBrun and R.D. Deslattes, Nucl. Instrum. Methods A347, 499 (1994).
[16] H. Aksela, S. Aksela, H. Pulkkinen, G.M. Bancroft, and K.H. Tan, Phys. Rev. A 37, 1798 (1988).
[17] M. Meyer, E.v. Raven, B. Sonntag, and J.E. Hansen, Phys. Rev. A 43, 177 (1991).
[18] J.A. de Gouw, J. van Eck, J. van der Weg, and H.G.M. Heideman, J. Phys. B: At. Mol. Opt. Phys. 25, 2007 (1992).
[19] H. Pulkkinen, S. Aksela, O.-P. Sairanen, A. Hiltunen, and A. Aksela, J. Phys. B: At. Mol. Opt. Phys. 29, 3033 (1996).
[20] J.W. Cooper, S.H. Southworth, M.A. MacDonald and T. LeBrun, Phys. Rev. A 50, 405 (1994).

different manifolds of states are involved. Second, a vacancy cascade spectrum was also recorded 63.1 eV above threshold to investigate the effects of producing KM-double vacancies in the initial photoionization step (Deslattes[21 22 23], Deslattes *et al.*[24]). The 63.1 eV spectrum (not shown here) is very similar to the 4.9 eV spectrum (1B) and transitions involving KM-double vacancies in the initial states could not be observed. Third, the strong $L_{2,3}$-$M_{2,3}M_{2,3}$ peaks in the 200-210 eV range of spectrum 1A are also observed on top of background in the vacancy-cascade spectra (Fig. 1B) recorded above threshold. These transitions result from $L_{2,3}$ vacancies produced either by direct photoionization or by Kα fluorescence following K-shell photoionization and will be discussed below with regard to coincidence measurements. Busch *et al.*[11] give a ratio for the production of holes above threshold of K:L_1:$L_{2,3}$ = 1:0.06:0.03 and Kochur and Sukhorukov[13] give 0.92:0.06:0.03. The yield for the Kα process is about 10% (Kochur *et al.*[7]), which means that about 25 % of the intensity of the normal $L_{2,3}$-$M_{2,3}M_{2,3}$ Auger-transitions in fig. 1B can be attributed to direct 2p photoionization and ≈ 75 % due to Kα fluorescence.

Our own Hartree-Fock calculations on $L_{2,3}$-MM Auger-transitions in the presence of spectator holes agree well with the results of Busch *et al.*[11]: spectator holes in the L(M) shell increase(decrease) the transition energy compared to the transitions with only one 2p vacancy in the initial state, and more complex multiplets broaden the structures. In addition, for the resonant case, there are always strong shake-up channels in the transitions from single to double hole states.

---

[21] R.D. Deslattes, Phys. Rev. 133, A390 (1964).
[22] R.D. Deslattes, Phys. Rev. 133, A399 (1964).
[23] R.D. Deslattes, Aust. J. Phys. 39, 845 (1986).
[24] R.D. Deslattes, R.E. LaVilla, P.L. Cowan, and A. Henins, Phys. Rev. A 27, 923 (1983).

However, while general features of these vacancy-cascade spectra can be explained using atomic structure calculations, the overlap between transitions in different decay pathways makes detailed analysis very challenging if not impossible[7 9 10 11 13].

Coincidence techniques[25] provide a way to choose a subset of transitions in order to disentangle the complicated vacancy cascade. Cooper[26] showed how electron-electron coincidence methods were applied *e.g.* by Raven *et al.*[27] to disentangle cascade spectra in Ne, Ar, Kr and Xe. Cooper also included an analysis on angular correlations for this kind of experiment. Levin *et al.*[2] and Armen *et al.*[28] studied resonance and threshold effects in argon ion-yields measured coincident with K-LL and K-LM Auger-electrons. Hayashi *et al.*[6] and Kjeldsen *et al.*[12] measured threshold electrons in coincidence with ion charge states following photoexcitation/ionization across the Ar K-edge.

The approach described here is to record electron spectra in coincidence with fluorescent x-rays. Fig. 2 illustrates the decay cascade in a simple single-configuration Hartree-Fock model. The arrows in figure 2 indicate the decay pathway investigated here from the K hole state through Kα fluorescence to the 2p hole state, followed by $L_{2,3}$-MM Auger-decay into a double hole state in the M shell. The other pathway indicated is the most probable one: K-$L_{2,3}L_{2,3}$ Auger-decay into a double hole state in the 2p shell and then the subsequent decays into the M shell. We did not include all possible transitions for reasons of clarity. We also note that the energy levels in fig. 2 are simple configuration average energies. When the exciting photon beam is tuned to the energy of the discrete

---

[25]G. Stefani, L. Avaldi, and R. Camilloni, in *New Directions in Research with Third-Generation Soft X-Ray Synchrotron Radiation Sources*, edited by A.S. Schlachter and F.J. Wuilleumier (Kluwer, Dordrecht, 1994), p. 161.
[26]J.W. Cooper, in *Atomic Physics at High Brilliance Synchrotron Sources*, edited by H.G. Berry, P. Cowan, and D. Gemmell (Argonne, DOE, 1994), p. 251.
[27]E. v. Raven, Ph.D. thesis, University of Hamburg, Hamburg, 1992; E. v. Raven, M. Meyer, M. Pahler, and B. Sonntag, J. Electron. Spectrosc. Relat. Phenom. 52, 677 (1990).
[28]G.B. Armen, J.C. Levin, and I.A. Sellin, Phys. Rev. A 53, 772 (1996).

1s → 4p resonance, this coincidence technique selects a [Ar] $2p^{-1}4p$ initial state for the Auger-decay with the same parity as the ground state, which can not be reached by direct dipole excitation.

Auger-decays[29 30] are often treated in a static picture which is independent of the excitation process[17 31], but this assumption breaks down close to threshold due to the strong interaction between the primary ejected electron and Auger-electron. This post-collision interaction (PCI) was first observed using charged particles as PCI inducers[32 33 34] and has been studied both experimentally[35 36 37 38 39] and theoretically[40 41 42 43].The first experiments using photons to study PCI between photoelectrons and Auger-electrons were performed by Schmidt *et al.*[44]. Later, a first experiment on the angular dependence of PCI was performed[45]. Here we report PCI shifts observed in our coincidence experiment for the novel case of L_{23}-$M_{23}M_{23}$ Auger-electrons interacting with 1s photoelectrons. Comparison is made with PCI shifts measured near the 2p threshold[46 47] and with theoretical models[41 43].

---

[29]P. Auger, J. Phys. Radium. 6, 205 (1925).
[30]G. Wentzel, Z. Phys. 43, 524 (1927).
[31]W. Mehlhorn, in *Atomic Inner-Shell Physics*, edited by B. Crasemann (Plenum, New York, 1985), p. 119.
[32]K. Helenelund, S. Hedman, L. Asplund, U. Gelius, and K. Siegbahn, Phys. Scripta 27, 245 (1983).
[33]D. Gråf and W. Hink, J. Phys. B: at. Mol. Phys. 19, L221 (1986).
[34]R. Huster, W. Sandner, and W. Mehlhorn, J. Phys. B: At. Mol. Phys. 20 L287 (1987).
[35]L.O. Werme, T. Bergmark, and K. Siegbahn, Phys. Scripta 8, 149 (1973).
[36]E.J. McGuire, Phys. Rev. A 11, 1880 (1975).
[37]L. Asplund, P. Kelfve, B. Blomster, H. Siegbahn, and K. Siegbahn, Phys. Scripta 16, 268 (1977).
[38]H. Aksela, S. Aksela, H. Pulkkinen, G.M. Bancroft, and K.H. Tan, Phys. Rev. A 37, 1798 (1988).
[39] W. Eberhardt, S. Bernstorff, H.W. Jochims, S.B. Whitfield, and B. Crasemann, Phys. Rev. A 38, 3808 (1988).
[40]A. Niehaus, J. Phys. B: Atom. Molec. Phys. 10, 1845 (1977).
[41]P. van der Straten, R. Morgenstern, and A. Niehaus, Z. Phys. D 8, 35 (1988).
[42]M. Yu. Kuchiev and S.A. Sheinerman, Zh. Eksp. Teor. Fiz. 90, 1680 (1986).
[43]G.B. Armen, Phys. Rev. A 37, 995 (1988).
[44]V. Schmidt, N. Sandner, W. Mehlhorn, M.Y. Adam, and F. Wuilleмier, Phys. Rev. Lett. 38, 63 (1977).
[45]B. Kämmerling, B. Krässig, and V. Schmidt, J. Phys. B: At. Mol. Opt. Phys. 26, 261 (1993).
[46]H. Hanashiro, Y. Suzuki, T. Sasaki, A. Mikuni, T. Takayanagi, K. Wakiya, H. Suzuki, A. Danjo, T. Hino, and S. Ohtani, J. Phys. B: Atom. Molec. Phys. 12, L775 (1979).
[47]J.A. de Gouw, J. van Eck, H.G.M. Heidemann, J. Phys. B: At. Mol. Opt. Phys. 25, 2007 (1992).

II. Experiment

The experiments were carried out at beamline X24A[48] at the National Synchrotron Light Source. At this x-ray beamline, synchrotron radiation emitted by electrons passing through a bending magnet is collimated, dispersed using a double crystal monochromator and refocused into the interaction chamber. This beamline delivers a flux in the order of 10^{11} photons per second in a bandpass of roughly 0.8 eV (FWHM) into a 1×1 mm^2 spot using Si(111) crystals in the vicinity of the argon K-edge (E_K[Ar] = 3206.3 ± 0.3 eV[49]).

The x-ray beam is crossed with an effusive jet of argon atoms at the source point of a cylindrical mirror analyzer (CMA)[15]. The ultrahigh vacuum of the windowless beamline is separated by a 12.5 μm polypropylene foil from the higher pressure in the experimental chamber.

The CMA is mounted with its symmetry axis parallel to the polarization vector $\vec{P} = (0,0,P_z)$ of the incoming photons and accepts a cone of electrons emitted over angles $\alpha = 42.3° \pm 6°$ relative to $\vec{P}$. The electron analyzer was operated in retarding mode at 20 eV pass energy, resulting in an electron energy resolution of ≈ 0.5 eV (FWHM). The argon $L_{2,3}$-MM Auger-electrons were detected over the kinetic energy range 198-211 eV in the non-resonant case and over 202-215 eV for the 1s → 4p resonant case in 0.1 eV steps. The increase in retarding potential with kinetic energy reduces the effective source volume of the CMA, but since electron spectra were measured over a relatively small energy range, the influence of this effect on relative intensities is expected to be small.

---

[48] P.L. Cowan S. Brennan, R.D. Deslattes, A. Henins, T. Jach and E.G. Kessler, Nucl. Instrum. Methods A246, 154 (1986).
[49] M. Breinig, M.H. Chen, G.E. Ice, F. Parente, B. Crasemann, and G.S. Brown, Phys. Rev. A 22, 520 (1980).

A Si(Li) detector was positioned opposite the CMA to detect unresolved Kα (2p – 1s) and Kβ (3p – 1s) x-ray fluorescence, and was used to record in coincidence the subset of $L_{2,3}$-$M_{2,3}M_{2,3}$ Auger-transitions which follow the Kα radiative decay of the initially created 1s vacancy states. The contributions of $L_{2,3}$-$M_{2,3}M_{2,3}$ Auger-transitions which follow K Auger-decays and direct L shell photoionization were thereby excluded.

Both the CMA and Si(Li) outputs underwent pulse conditioning and were fed into a time-to-amplitude converter (TAC). The TAC output was recorded in a multi-channel analyzer (MCA) by defining two regions of interest (ROI): one over the "true" coincidence peak with the "random" background and one over purely "random" background in a different time region (see *e.g.* Stefani *et al.*[25]). While the kinetic energy was scanned, events in the ROI's were transferred as counts to the data-collection computer. Three different electron spectra were measured simultaneously: total electron counts, "true+random" coincidences and "random" coincidences. The "true" coincidence counts can be derived by subtracting the "random" coincidences from the "true+random" coincidences weighted with the width of the ROI's. The random coincidences spectra were identical, within statistical variations, to the non-coincident electron spectra (in fact, the product of the total photon and the total electron counts is proportional to the "random" coincidence counts). Thus, to reduce statistical errors, a properly normalized non-coincident electron spectrum was subtracted from the "true+random" coincidences instead of the "random" coincidence spectrum itself.

Using this technique, we select the subset of $L_{2,3}$-$M_{2,3}M_{2,3}$ Auger-transitions which are correlated with Kα fluorescence decays; all others, such as following K Auger-decays or direct 2p photoionization, are excluded. Kochur *et al.*[7] presented a calculation for the decay of the 1s hole in argon, showing that 11% of the 1s holes will decay through Kα

fluorescence, 1% through Kβ fluorescence and 88% through K Augers. The unresolved detection of the Kβ fluorescence only contributes to the "random" background, because it is not correlated with $L_{2,3}$-$M_{2,3}M_{2,3}$ electron emission.

The photon energy calibration was established by scanning through the argon K-edge and recording the position of the prominent argon 1s → 4p resonance (E(1s → 4p) = 3203.6 ± 0.3 eV [49]) in the fluorescence yield with the Si(Li) detector. The kinetic energy calibration of the CMA was determined by reducing the x-ray energy 30 eV below the 1s → 4p resonance and then recording a "normal" Ar $L_{2,3}$-$M_{2,3}M_{2,3}$ Auger-spectrum. At this photon energy (≈ 3174 eV), $L_{2,3}$ photoelectrons are ejected with ≈ 2925 eV kinetic energy, so PCI effects are expected to be negligible. The transition energies reported by Werme *et al.*[35] were used to calibrate our Auger-spectra. We interpret measured peak shifts relative to this below-threshold spectrum as due to changes in screening by the 4p spectator electron or due to PCI shifts involving the 1s photoelectron.

III. Results & Discussion

In fig. 3 are plotted low-resolution (ΔE ≈ 4eV) $L_{2,3}$-MM electron and coincidence spectra recorded over the 120 - 240 eV kinetic energy range at x-ray energies 30 eV below the 1s → 4p resonance (Fig. 3A), 10 eV above the K-ionization threshold (Fig. 3B), and on the 1s → 4p resonance (Fig. 3C). The electron spectra in fig. 3 are essentially low resolution versions of those in fig.1, except that coincidence spectra were also recorded.

The low-resolution data in fig. 3 demonstrate three aspects of the selectivity of the coincidence method. First, many of the transitions appearing in the non-coincident spectra

recorded on the 4p resonance or above the K-threshold are eliminated in the coincidence spectra due to the exclusion of vacancy-cascade pathways which start with K-LL or K-LM Auger-emission. Second, since K-L_1 x-ray emission is dipole forbidden and all L-shell vacancies produced by direct photoionization are excluded from the coincidence spectra, the L_{23} vacancies produced by L_1-L_{23}M transitions are eliminated. This explains why the strong satellites which overlap the L_{23}-M_1M_{23} transitions[20] (kinetic energy range = 185 - 195 eV) in the electron spectrum recorded 30 eV below the 4p resonance (Fig. 1A and 3A) are greatly reduced in the coincidence spectra (Fig. 3B and C). Third, the strong L_{23}-$M_{23}M_{23}$ transitions observed in both the below-threshold spectrum (Fig. 3A) and the coincidence spectrum recorded 10 eV above threshold (Fig. 3B) are modified in the coincidence spectrum recorded on the 4p resonance (Fig. 3C). The corresponding transitions are shifted several eV higher in energy and have a different peak shape, i.e., the states involved in the vacancy cascade are modified by the 4p electron.

Fig. 4 shows electron spectra in the energy range of the Ar $L_{2,3}$-$M_{2,3}M_{2,3}$ Auger-transitions recorded with higher resolution to further investigate the spectra. For the spectrum in fig. 4A the photon energy was tuned to 32.7 eV below threshold, resulting in the well known "normal" spectrum[35] produced by direct photoionization of the $L_{2,3}$ subshells. The dashed lines in fig. 3B and C represent the non-coincident cascade spectra at 10 eV above the K-threshold and on the 1s → 4p resonance (similar to the spectra in fig. 1B and C) and the solid lines are the corresponding electron/x-ray coincidence spectra.

We observe two differences in comparing fig. 4A with the coincidence spectrum in fig. 4B:

1) the relative intensities of the structures are changed, and

2) the structures in Fig. 4B appear at slightly higher energies.

The intensity changes are caused by angular correlation effects in the coincidence measurement as shown by Arp *et al.*[50]. The predicted intensity changes, which depend on the direction in which the fluorescence photon is detected relative to the CMA symmetry axis, are in good agreement with the intensity changes observed in our experiment. The energy shifts are attributed to the influence of post-collision interaction with the 1s photoelectron and are discussed in section C below.

The coincidence spectrum in fig. 4C was obtained using photons tuned to the 1s - 4p resonance. The differences between this coincidence spectrum and the "normal" spectrum in fig. 4A are even stronger:

1) the Auger-transitions in fig. 3C show a strong resonance shift,

2) the lines are broader, and

3) additional structures appear on the low energy side of the spectrum.

These effects are apparently due to the presence of the 4p electron and were investigated by comparison with model spectra constructed using atomic structure calculations.

A. Non-resonant coincidence spectra and comparison to Hartree-Fock calculations

To interpret the coincidence spectra, a single-configuration Hartree-Fock (SCHF) calculation, utilizing Cowan's[51] codes, was performed. First, the population of the two

[50]U. Arp, J.W. Cooper, T. LeBrun, S.H. Southworth, M. Jung, and M.A. MacDonald, accepted by J. Phys. B: At. Mol. Opt. Phys.
[51]R.D. Cowan, *The Theory of Atomic Structure and Spectra* (University of California Press, Berkeley, 1981).

states in the configuration [Ar] $2p^{-1}$ produced by Kα fluorescence was calculated. Despite relativistic corrections in the programs, the result was an exact 2:1 ratio for the number of L_3 to L_2 holes. Then, the difference in the configuration average energies for the initial and final ionic states for the $L_{2,3}$-$M_{2,3}M_{2,3}$ Auger-transitions was determined: $\Delta E_{av} = E_{av}([Ar]\ 2p^{-1}) - E_{av}([Ar]\ 3p^{-2})$. The multiplet splitting of the final and initial states was also deduced from that calculation by combining energy values for the electron-electron (Slater integrals G^K and F^K) and spin-orbit interaction. Combining the multiplet splitting with the difference in the configuration average energies then gave the transition energies.

A calculation for the Auger transition rates was done in which ΔE_{av} was the kinetic energy ε_A of the Auger electron. This approach neglects the energy dependence of the continuum wave functions for different final states, but taking into account the relatively high kinetic energies and the small energy variations for the various final states, this assumption seems reasonable. A similar approach was adopted by Meyer *et al.*[17]. The radial Coulomb matrix elements $R^0(3p3p, 2p\varepsilon_A p)$, $R^2(3p3p, 2p\varepsilon_A p)$ and $R^2(3p3p, 2p\varepsilon_A f)$ were calculated to determine the transition strengths into the various final states. The combination of the five final states [Ar] $3p^{-2}\ ^3P_0$, $^1S_0$, $^3P_1$, $^3P_2$, $^1D_2$ and the two initial states [Ar] $2p^{-1}\ ^2P^\circ_{1/2}$ and $^2P^\circ_{3/2}$ results in ten transitions. Considering that we neglected configuration interaction (CI) in our SCHF calculation, the relative energies of the transitions were not correct. Following Meyer *et al.*[17], we used scaling of the Slater integrals to 85 % of their original values (see also Cowan[51] p. 464). This results in reasonable agreement between experiment and calculation, as seen in fig. 5, except for the position of the L_3-$M_{23}M_{23}$ $^1S_0$ line, the relative intensities of the two major peaks, and the width of the L_2-$M_{23}M_{23}$ $^3P_{0,1,2}$ triplet. The calculated spectrum has been shifted by δE_{calc} = -0.7 eV to

align with experimental energies and normalized to the same area under the curves. The calculated curve was generated from the line spectrum by convolution with a Lorentzian to account for the finite lifetime of the $L_{2,3}$ core hole (FWHM = 0.13 eV[52]) and then convolution with a Gaussian (FWHM = 0.5 eV) to account for the resolution of the CMA.

Exact reproduction of the "normal" $L_{2,3}$-MM spectrum is complicated as shown before by Dyall and Larkins[53], who used initial and final state configuration interaction in order to calculate the energies and intensities of the transitions correctly. But their multiplet splitting in the configuration [Ar] $3p^{-2}$ was still too big. Kvalheim[54] made an approach using a more complete basis set in his CI calculation, and his results were even closer to the experimental results. Cooper *et al.*[20] concluded in their investigation that the $L_{2,3}$-MM Auger spectrum of argon is still not completely understood.

B. Resonant coincidence spectra and comparison to Hartree-Fock calculations

The coincidence spectrum recorded at the 1s - 4p excitation was modeled under the assumption that the 4p electron acts as a "spectator" in the radiative and Auger-transitions. The result of these calculations is shown in fig. 6. The normal "spectator" spectrum was calculated in the same way as described above only that we have nine initial states for the Auger processes ([Ar] $2p^{-1}$ 4p $^1S_0$, $^3P_0$, $^3S_1$, $^1P_1$, $^3D_1$, $^3P_1$, $^1D_2$, $^3P_2$, $^3D_2$; for the different populations after the fluorescence decay see table 1). Together with the 21 final

[52]G.C. King and F.H. Read, in *Atomic Inner-Shell Physics*, edited by B. Crasemann (Plenum, New York, 1985), p. 317.
[53]K.G. Dyall and F.P. Larkins, J. Phys. B: At. Mol. Opt. Phys. 15, 2793 (1982).
[54]O.M. Kvalheim, Chem. Phys. Lett. 98, 457 (1983).

states in the configuration [Ar] $3p^{-2}$ 4p we get 189 normal transitions, not considering shake processes.

The spectrum with the "4p-spectator"-electron is shifted to higher energies, the structures are broadened and there are additional structures. The first difference is called resonance shift and is mainly due to a change in the binding energy of the loosely bound 4p-electron during the transition from a singly-charged [Ar] $2p^{-1}$ 4p to a doubly-charged [Ar] $3p^{-2}$ 4p core. The broadening is caused by the more complicated multiplet structure due to the interaction of the unpaired 4p electron with the ionic core. We interpret the additional structures on the low energy side to result from 4p → 5p shake transitions (Aksela *et al.*[38], Meyer *et al.*[17]).

The total shake probability in an Auger transition can be estimated by calculating the radial overlap between the wavefunctions of the two involved configurations (see *e.g.* Åberg[55], Meyer *et al.*[17])

$$P_{if}([Ar]2p^{-1}4p,[Ar]3p^{-2}4p) = \langle 1s^{\bullet}|1s\rangle^2 \langle 2s^{\bullet}|2s\rangle^2 \langle 2p^{\bullet}|2p\rangle^5 \langle 3s^{\bullet}|3s\rangle^2 \langle 3p^{\bullet}|3p\rangle^4 \langle 4p^{\bullet}|4p\rangle \qquad (1)$$

where $\langle nl^{\bullet}|$ is taken from the initial state and $|nl\rangle$ from the final state configuration. This leads to a total estimated shake-up probability of $1 - P_{if}^2 \approx 20$ % for the transitions [Ar] $2p^{-1}$ 4p into [Ar] $3p^{-2}$ 4p. The values for the calculated overlap integrals are listed in table 2. In comparison with values for the non-resonant Auger-process, also listed in table 2, it is demonstrated that the strong shake-up channel in the calculated spectrum is completely caused by relaxation of the loosely bound 4p-electron.

It is also possible to estimate the strength of shake-up transitions using equation (1).

---

[55]T. Åberg, Phys. Rev. 156, 35 (1967).

For example, in order to estimate the strength of the shake-up transitions from [Ar] $2p^{-1}$ 4p into [Ar] $3p^{-2}$ 5p one has to calculate the overlap matrix elements between these two configurations

$$P_{if}([Ar]2p^{-1}\,4p,[Ar]3p^{-2}5p) = \langle 1s^{*}|1s\rangle^{2}\langle 2s^{*}|2s\rangle^{2}\langle 2p^{*}|2p\rangle^{5}\langle 3s^{*}|3s\rangle^{2}\langle 3p^{*}|3p\rangle^{4}\langle 4p^{*}|5p\rangle \qquad (2)$$

This approach, which Meyer *et al.*[17] called the projection of the initial state wavefunction on the final state wavefunction, leads to an estimated shake-up probability P_{if}^{2} into [Ar] $3p^{-2}$ 5p of 19 %. Shake transitions into states of the configurations [Ar] $3p^{-2}$ np, n > 5 do not play an important role, as shown in table 3. For some higher initial Rydberg-states (6p, 7p) shake-processes are predicted to dominate the Auger-spectra, as seen in the case of the 2p → nd series by Meyer *et al.*[17].

It should be noted that, due to the lifetime broadening of K vacancies (≈ 0.68 eV, Krause and Olivier[67], Kochur *et al.*[7]), it is possible that small amounts of [Ar] $2p^{-1}$5p states are produced from the initial excitation, as suggested by Breinig *et al.*'s[49] absorption spectrum.

In addition, according to the scattering theory model (Åberg and Craseman[14], Armen *et al.*[28]) the 1s → np, n = 4,5,6... Rydberg and threshold continuum states participate as coherently excited intermediate states in the photoexcitation/decay process, so the quantum number of the initially excited 1s electron is not well defined. However, treatment of the 1s → 4p excitation as an isolated resonance appears to be adequate in the present experiment.

The calculated results for the Auger-decay of [Ar] $2p^{-1}$ 4p are shown in fig. 6 in comparison with the coincidence spectrum measured on the 1s → 4p resonance. As in the non-resonant case, scaling of the Slater integrals to 85 % of their original values was

applied. The calculated spectrum was also shifted by δE_{calc} = -0.7 eV to align with experimental energies and normalized to the same area under the curve. The relative energy positions are not in complete agreement with experiment and also the relative intensities agree only fairly. The vertical bars above the spectrum are included to distinguish between normal "spectator" transitions, where the 4p electron remains in its orbital, and the transitions in which the 4p electron is "shaken-up" into a 5p state. The strength of the shake-up transitions is apparently underestimated by the calculation, which is not surprising since a simple overlap model for the shake processes was applied. Also, as noted above, initially-excited 5p spectator states may contribute, but the estimated energy range for Auger-transitions [Ar] $2p^{-1}5p$ into [Ar] $3p^{-2}5p$ is ≈ 206 - 213 eV, which is too high to explain all discrepancies on the low energy side.

C. Post-collision interaction

For argon K-shell photoionization PCI would usually be studied between the 1s photoelectron and the K Auger-electrons, however the K Auger-decay channels are excluded in our coincidence data. We have observed the effect of elimination of PCI between 1s photoelectrons and K Auger-electrons in 1s photoelectron/x-ray coincidence spectra, discussed in refs.[9 10 15]. Here we study the PCI between 1s photoelectrons and $L_{2,3}$-$M_{2,3}M_{2,3}$ Auger-electrons following Kα x-ray emission.

In addition to the comparison between resonant and non-resonant Auger-spectra in the coincidence experiment, we also measured non-resonant spectra at several excess

energies $E_t = h\omega - E_K$ above threshold. The idea was to study PCI in the coincidence experiment and compare it to theory and other measurements made in the vicinity of the 2p thresholds. There are several interesting differences between PCI in the coincidence experiment and "normal" PCI:

A) The photoelectron has p symmetry in the coincidence experiment, because the 1s shell is photoionized, and d or s symmetry when the 2p shell is photoionized. This causes different photoelectron angular distributions (see *e.g.* Scofield[56] [57], Bechler and Pratt [58] [59], Cooper[60] [61] [62], Krässig *et al.* [63], Jung *et al.*[64], and Shaw *et al.* [65]).

B) Due to angular correlation effects in the coincidence experiment, we observe an anisotropic angular distribution of L_3-MM Auger-transitions, which will influence the strength of PCI, even when measured in the angular average (see Arp *et al.*[50] for details).

C) In semi-classical models of PCI, the strength of the interaction depends on the time delay between the photoelectron and Auger-electron emissions. In the "normal" Auger-decay this is just the lifetime of the 2p core-level τ_{2p}, whereas in the coincident case the effective lifetime is $\tau_{eff} = \tau_{2p} + \tau_{1s}$.

Our experimental values for the $L_{2,3}$-$M_{2,3}M_{2,3}$ line positions were determined through a fitting procedure, in which the sum of five Voigt-profiles was fitted to the spectra. These fits were made to spectra measured in coincidence above the K threshold and to "normal" spectra measured below the K-edge. Then the differences in the energy positions were

---

[56] J.H. Scofield, Phys. Rev. A 40, 3054 (1989).
[57] J.H. Scolfield, Phys. Scripta 41, 59 (1990).
[58] A. Bechler and R.H. Pratt, Phys. Rev. A 39, 1774 (1989).
[59] A. Bechler and R.H. Pratt, Phys. Rev. A 42, 6400 (1990).
[60] J.W. Cooper, Phys. Rev. A 42, 6942 (1990).
[61] J.W. Cooper, Phys. Rev. A 45, 3362 (1990).
[62] J.W. Cooper, Phys. Rev. A 47, 1841 (1993).
[63] B. Krässig, M. Jung, D.S. Gemmell, E.P. Kanter, T. LeBrun, S.H. Southworth, and L. Young, Phys. Rev. Lett. 75, 4736 (1995).
[64] M. Jung, B. Krässig, D.S. Gemmell, E.P. Kanter, T. LeBrun, S.H. Southworth, and L. Young, Phys. Rev. A 54, 2127 (1996).
[65] P.S. Shaw, U. Arp, and S.H. Southworth, Phys. Rev. A 54, 1463 (1996).

determined for all five profiles and the average was used as the measured difference. These values are listed in table 4 and plotted in fig. 7. The combined standard error in the measured values was determined from the statistical errors in the fits and an estimated error of ± 0.04 eV from the uncertainty in the energy calibration and time stability of the incident x-ray beam energy. The resulting total errors are listed in column 3 of table 4.

To compare with theoretical approaches, the bandpass of the CMA has to be taken into account. Very simple estimations for line shifts would lead to incorrect results in this case, where the energy position of the line maximum is changed by the convolution with the detector bandpass, mainly because PCI profiles are highly asymmetric and can have a long tail on the high energy side. For simple estimations of the shift in the line maximum see *e.g.* Straten *et al.*[41].

Two theoretical models were applied: the classical approach goes back to Niehaus and Zwakhals[66] and Helenelund *et al.*[32], and we follow the formulation of Straten *et al.*[41]. The quantum mechanical approach is based on Kuchiev and Sheinerman's[42] work, and we use the formulation given by Armen[43].

Both approaches produce a PCI distorted Auger-line for each excess energy E_1 which we then convoluted with a Gaussian of width 0.5 eV to account for the bandpass of the CMA. The strength of PCI depends on the lifetime of the initial state hole $\tau = \hbar/\Gamma$. This lifetime results in a time delay between the emission of the photoelectron and the Auger-electron; here the effective time delay is the sum of the lifetimes of the 1s and 2p coreholes $\tau_{eff} = \tau_{2p} + \tau_{1s}$. The tabulated lifetime widths are: $\Gamma_{2p} = 0.12$ eV[14] and $\Gamma_{1s} = 0.68$[67], leading to an effective core-level width $\Gamma_{eff} = 0.109$ eV in the coincidence experiment.

---

[66] A. Niehaus and C.J. Zwakhals, J. Phys. B 16, L135 (2977).
[67] M.O. Krause and J.H. Olivier, J. Phys. Chem. Ref. Data 8, 329 (1979).

Voigt-profiles were then fitted to the calculated, convoluted profiles and the resulting energy positions used as "theoretical" shifts. These shifts are listed in table 4 and plotted in fig. 6 along with the experimental results of Hanashiro *et al.*[46] and de Gouw *et al.*[47] who both measured PCI shifts in the L_{23}-$M_{23}M_{23}$ Auger-transitions at photon energies close to the 2p thresholds. In addition, model calculations for de Gouw *et al.*'s high resolution spectra ($\Delta E = 0.1$ eV) using both Straten *et al.*'s[41] and Armen's[43] approaches are shown, performed using the same method described before.

The large error bars on Hanashiro *et al.*'s[46] data (filled boxes) make an interpretation very difficult. Our data (filled circles) are consistently lower than the corresponding values deduced from the model calculations (open circles and boxes), suggesting a systematic discrepancy between experiment and calculation. The same disagreement persists for the data of de Gouw *et al.*[47] (filled triangles) and their calculated equivalents (open triangles), but the difference is smaller. Remarkable is the negative shift measured at 297.3 eV excess energy, which is predicted to occur in angle-resolved PCI measurements[41 43].

The parameter C in Straten *et al.*'s treatment is angle-dependent. We used their expression for an isotropic angular distribution, which is only correct for a magic angle CMA and a non-coincident experiment (see appendix A for details). In this coincidence experiment we expect angular correlation effects to influence the spectra as shown by Arp *et al.*[50]. A more detailed analysis of angular effects in PCI, influence of angular correlation and the role of non-dipole contributions in photoelectron angular distributions given in appendix A.

Several factors which are not included in the current PCI theory can contribute to the discrepancies with the measured energy shifts:

A. Total neglect of the recoil ion in the PCI treatment, because only the interaction

between the two electrons is included in the theoretical treatment of PCI and the influence of the third particle is completely neglected. But if an expansion of PCI models in this direction would help to explain the discrepancies reported here is not clear.

B. Non-dipole effects in the photoelectron angular distribution[18] (van Straten *et al.*[41] assumed a pure dipole angular distribution in their treatment),

C. Angular correlation effects in the coincidence experiment (Arp *et al.*[50]).

The influence of non-dipole effects and angular correlation is analyzed in appendix A and does not help to explain these discrepancies.

So this systematic difference persists also after a thorough analysis and has probably to be attributed to the low statistics in the experiment.

Conclusion

Ar $L_{2,3}$-$M_{2,3}M_{2,3}$ Auger-electron spectra measured in coincidence with Kα fluorescence photons after 1s photoionization/excitation have been reported here. The coincidence spectra are greatly simplified in comparison with conventional electron spectra, allowing a more detailed analysis of the vacancy cascade process.

A single configuration Hartree-Fock calculation agrees well with the Auger-spectrum measured after 1s photoionization when the calculated spectrum is shifted in energy by -0.7 eV and the Slater-integrals are scaled to 85 % of the *ab initio* values. The calculation of the Auger-electron spectrum after resonant 1s – 4p photoexcitation is more complicated and the resulting agreement is only fair. Here, shake-up transitions are important, but are only qualitatively accounted for in the calculations.

Post-collision induced energy shifts were measured for cascade Auger-electrons, but comparison with calculated shifts indicates that further theoretical analysis and higher-resolution measurements are needed.

Acknowledgments

The authors thank B.A. Karlin for technical assistance and Drs. T.D. Thomas and G.B. Armen for sharing their knowledge on PCI with us. UA thanks the Alexander von Humboldt-foundation for financial support and Dr. R.D. Deslattes and the members of the Quantum Metrology Division of the National Institute of Standards and Technology for their kind hospitality.

Measurements were made at the National Synchrotron Light Source, Brookhaven National Laboratory, which is supported by the U.S. Department of Energy, Divisions of Materials and Chemical Sciences.

This work was supported by the U.S. Department of Energy Office of Basic Sciences under contract W-31-109-Eng-38.

Appendix A: Angular dependence of PCI, non-dipole effects and alignment.

Straten *et al.*[41] use the following formulation in atomic units for the PCI profile:

$$P(\varepsilon) \propto \frac{\exp\left(2\sqrt{2}\,\mathrm{Im}(\phi(z^*))\right)}{\left\{\left(E_1+\frac{\varepsilon}{C}\right)^2+\frac{\Gamma^2}{4}\left(1+\frac{1}{C}\right)^2\right\}^{\frac{1}{4}}\left(\varepsilon^2+\frac{\Gamma^2}{4}\right)} \qquad \textbf{(A.1)}$$

where ε is the actual kinetic energy of the Auger-electron after the distortion by PCI, Γ is the lifetime of the initial state, and with the point of stationary phase z^*

$$z^* = \frac{1}{R^*} = \frac{\varepsilon+\frac{i\Gamma}{2}}{C} \qquad \textbf{(A.2)}$$

and the abbreviation C

$$C = 1-\frac{|\vec{v}_1|}{|\vec{v}_A-\vec{v}_1|} \qquad \textbf{(A.3)}$$

where v_A is the velocity of the Auger-electron and v_1 that of the photoelectron, and the function $\phi(z^*)$

$$\begin{aligned}\phi(z^*) = {} & I\left(E_i, E_1+\frac{i\Gamma}{2}, 1\right) - I\left(z^*, E_1+\frac{i\Gamma}{2}, 1\right) \\ & -I(E_i, E_1-\varepsilon, 1+C) + I(z^*, E_1-\varepsilon, 1+C)\end{aligned} \qquad \textbf{(A.4)}$$

with

$$I(z,E,x) = \frac{(E+xz)^{\frac{1}{2}}}{z} - \frac{x}{2\sqrt{E}} \ln\left(\frac{(E+xz)^{\frac{1}{2}} - E^{\frac{1}{2}}}{(E+xz)^{\frac{1}{2}} + E^{\frac{1}{2}}} \right) \qquad \textbf{(A.5)}$$

The angular dependence of PCI is contained in the parameter C depending on the velocities of the two electrons $\vec{v}_1 = (v_1,\theta,\phi)$ and $\vec{v}_A = (v_A,\theta',\phi')$. This formulation applies to an electron-electron coincidence experiment in which both electrons are detected angle dependent and energy resolved. In experiments where the photoelectron is not detected C has to be multiplied by the differential photoionization cross section and integrated over the solid angle. Under the assumption that $\frac{d\vec{v}_1}{dt} = \frac{d\vec{v}_A}{dt} = 0$ (especially no deflection, which will be a very crude approximation if the angle between the two emission directions is small) we can apply an expansion of the Green's function in spherical harmonics (see *e.g.* Varshalovich *et al.*[68]):

$$\frac{1}{|\vec{v}_1 - \vec{v}_A|} = 4\pi \sum_{l=0}^{\infty} \sum_{m=-l}^{l} \frac{1}{2l+1} \frac{v_<^l}{v_>^{l+1}} Y^*_{l,m}(\theta',\phi') Y_{l,m}(\theta,\phi) \qquad \textbf{(A.6)}$$

with $v_< = \min(v_1,v_A)$ and $v_> = \max(v_1,v_A)$ and following the definition of Varshalovich *et al.*[68] for the phase relation between complex conjugate functions and applying the orthogonality relation allows us to perform the integration.

It is common to use the dipole approximation for the differential photoionization

[68]D.A. Vashalovich, A.N. Moskalev, and V.K. Khersonskii, *Quantum Theory of Angular Momentum* (World Scientific, Singapore, 1988), p. 130ff.

cross section, but it was predicted by Scofield[56 57], Bechler and Pratt[58 59] and Cooper[50 61 62] that non-dipole effects will affect the angular distribution of photoelectrons much earlier than the total cross section. This was also proven recently by Krässig *et al.*[63] and Jung *et al.*[64] who measured photoelectron angular distributions far above threshold for argon and krypton and found strong forward-backward asymmetries in good agreement with Cooper's calculations.

Shaw *et al.*[65] performed a thorough analysis on ways to determine these non-dipole asymmetries expanding Cooper's formulation for the case of not completely polarized light and showing that the cross section can be written as a cosine Fourier-series in the azimuthal angle ϕ leading to the following equation

$$\frac{d\sigma}{d\Omega}(\theta,\phi) = \frac{\sigma_{nl}}{4\pi}\left[\begin{array}{l} 1+\frac{\beta}{8}(1+3P)(3\cos(\theta)^2-1) \\ +\delta\sin(\theta)\cos(\phi)+\gamma\cos(\theta)^2\sin(\theta)\cos(\phi) \\ +\gamma\frac{(P-1)}{8}(5\cos(\theta)^2-1)\sin(\theta)\cos(\phi) \\ +\frac{3\beta}{8}(P-1)\sin(\theta)^2\cos(2\phi) \\ +\gamma\frac{P-1}{8}\sin(\theta)^3\cos(3\phi) \end{array}\right] \qquad \text{(A.7)}$$

in which β is the dipole asymmetry parameter, δ and γ are parameters describing the forward-backward asymmetry, P ($0 \leq P \leq 1$) is the degree of linear polarization as defined by Shaw *et al.*[65] and σ_{nl} is the total cross section.

The integration of eqn. (A.6) multiplied by eqn. (A.7) over the solid angle leads to the following results for the parameter $C(\theta', \phi')$, with $v = \sqrt{2E}$ in atomic units:

$$
\begin{aligned}
C(\theta',\phi') = 1 &- \sqrt{\frac{E_1}{E_A}} - \left(\frac{\delta}{3} - \frac{\gamma}{15}\right)\frac{E_1}{E_A}\sin(\theta')\cos(\phi') \\
&- \frac{\beta}{40}(1-3P)\left(\frac{E_1}{E_A}\right)^{\frac{3}{2}}(3\cos(\theta')^2-1) - \frac{3\beta}{40}(P-1)\left(\frac{E_1}{E_A}\right)^{\frac{3}{2}}\sin(\theta')^2\cos(2\phi') \\
&- \left(\frac{\gamma}{35} + \frac{\gamma}{56}(P-1)\right)\left(\frac{E_1}{E_A}\right)^{2}(5\cos(\theta')^2-1)\sin(\theta')\cos(\phi') \\
&- \frac{\gamma}{56}(P-1)\left(\frac{E_1}{E_A}\right)^{2}\sin(\theta')^3\cos(3\phi') \qquad \forall\ E_1 \le E_A
\end{aligned}
\tag{A.8}
$$

and

$$
\begin{aligned}
C(\theta',\phi') = &-\left(\frac{\delta}{3} + \frac{\gamma}{15}\right)\sqrt{\frac{E_A}{E_1}}\sin(\theta')\cos(\phi') \\
&- \frac{\beta}{40}(1+3P)\frac{E_A}{E_1}(3\cos(\theta')^2-1) - \frac{3\beta}{40}(P-1)\frac{E_A}{E_1}\sin(\theta')^2\cos(2\phi') \\
&- \left(\frac{\gamma}{35} + \frac{\gamma}{56}(P-1)\right)\left(\frac{E_A}{E_1}\right)^{\frac{3}{2}}(5\cos(\theta')^2-1)\sin(\theta')\cos(\phi') \\
&- \frac{\gamma}{56}(P-1)\left(\frac{E_A}{E_1}\right)^{\frac{3}{2}}\sin(\theta')^3\cos(3\phi') \qquad \forall\ E_1 \ge E_A
\end{aligned}
\tag{A.9}
$$

For $P = 1$, $\gamma = \delta = 0$ these results are the same as van der Straten *et al.*[41] have derived. They performed their calculation only for electron detection in a plane perpendicular to the photon beam, but our less restricted calculation leads to the same result. Armen[43] mentions that the probability for the emission of an Auger-electron in a certain direction in space has to be taken into account. Alignment effects of the residual ion after photoionization might cause anisotropies in the Auger-electron angular distribution if the total angular momentum of the initial state is larger than ½. Now we have to perform the same kind of integration again. It is assumed to be a good approximation that the Auger-electron angular distribution is isotropic.

If an electron detector with small acceptance angle is used and the Auger-electron angular distribution is isotropic we do not have to integrate equations (A.8) and (A.9), but can use them directly to determine the desired parameter.

However, one of the most commonly used electron detectors is a cylindrical mirror analyzer (CMA) accepting electrons under an angle $\rho \pm \Delta\rho$ relative to the polarization of the incoming radiation and over a full circle of the azimuthal angle η. In this case we have to integrate $C(\theta',\phi')$ multiplied with the differential cross section for the Auger-electron emission over the acceptance angles of the CMA.

With $\int_0^{2\pi} dx \cos(nx) = 0$ and an isotropic angular distribution for the Auger-electrons

all the terms in the integration of $C(\theta',\phi')$ coming in from higher order multipoles drop out and also the term coming from the unpolarized light leading to the following much simpler integrals and their approximations

$$C_{CMA} = \frac{\int_{\rho-\Delta\rho}^{\rho-\Delta\rho} d\theta' \sin(\theta') \left(1 - \sqrt{\frac{E_1}{E_A}} - \frac{\beta}{40}(1+3P)\left(\frac{E_1}{E_A}\right)^{\frac{3}{2}}(3\cos(\theta')^2-1) \right)}{\int_{\rho-\Delta\rho}^{\rho+\Delta\rho} d\theta' \sin(\theta')} \qquad \textbf{(A.10)}$$

$$\approx 1 - \sqrt{\frac{E_1}{E_A}} - \frac{\beta}{40}(1+3P)\left(\frac{E_1}{E_A}\right)^{\frac{3}{2}}(3\cos(\rho)^2-1) \qquad \forall\ E_1 \le E_A$$

and

$$C_{CMA} = \frac{\int_{\rho-\Delta\rho}^{\rho-\Delta\rho} d\theta' \sin(\theta') \left(-\frac{\beta}{40}(1-3P)\frac{E_A}{E_1}(3\cos(\theta')^2-1) \right)}{\int_{\rho-\Delta\rho}^{\rho-\Delta\rho} d\theta' \sin(\theta')} \qquad (A.11)$$

$$= -\frac{\beta}{40}(1+3P)\frac{E_A}{E_1}(3\cos(\rho)^2-1) \qquad \forall\ E_1 \geq E_A$$

If the CMA accepts only over a small angle $\pm \Delta\rho$ we arrive at exactly the same result as van der Straten *et al.*[41], except for the polarization dependence. Most CMAs accept electrons under the "dipole" magic angle $\rho = \text{acos}(\sqrt{1/3}) = 54°44'8''$. In that case the PCI vanishes when the photoelectron passes the Auger-electron ("no-passing effect"). In the case where the electrons are accepted under a different angle we might encounter negative PCI even in the angle average. Polarization less then 100% reduces the anisotropy effects considerably in this case, but they do not vanish completely as predicted by van der Straten *et al.*[41]. This is because if when unpolarized radiation is used the propagation direction of the photons becomes the quantization direction and the photoelectron angular distribution will not be symmetric.

That the non-dipole effects have no influence on C_{CMA} is not surprising, because they cause a forward-backward asymmetry which will average out when we integrate over ϕ from 0 to 2π. The same is true for the contribution from the unpolarized light. A very different result is to expect when the symmetry axis of the CMA is parallel to the propagation direction of the incoming photons, which is equivalent to a rotation of the coordinate system by 90° degrees around the y-axis; x=z', y=y' and z=-x' would have to be replaced in the equations, leading to much more interesting integration. Then all the non-

dipole and polarization effects would not average out and remain in the factor C_{CMA}. Now in the coincidence experiment we don not have isotropic Auger-electron angular distributions, as shown by Arp *et al.* [50]. Now $C(\theta',\phi')$ has to be integrated over the CMA acceptance angles multiplied with the Auger-electron angular distribution. The results for C if the photon is detected in z-direction and an anisotropic angular Auger-electron distribution caused by angular correlations are listed in table A.1. The difference compared to an isotropic angular distribution is very small and can not be the reason for the discrepancies in our experiment, but we have to note that at excess energies above the Auger-electron kinetic energy the parameter C can become negative in our case, because the used CMA does not accept electrons under the dipole magic angle.

This review of angular effects in PCI was done for Straten *et al.*'s[41] formulation, but the same applies for the model used by Armen[43], where the angular dependence is contained in the parameter $\xi = C \cdot v_1^{-1}$.

This work was supported by the U.S. Department of Energy, Office of Basic Energy Sciences, under contract W-31-109-ENG-38.

Tables and table captions.

Table I. Calculated population of the different states in the configuration [Ar] $2p^{-1}$ 4p after Kα fluorescence following resonant 1s – 4p excitation.

Final state [Ar] $2p^{-1}$ 4p	Relative population in %
$^1S_0$	8.23
$^3P_0$	2.89
$^3S_1$	4.32
$^1P_1$	19.35
$^3D_1$	5.05
$^3P_1$	4.62
$^1D_2$	18.49
$^3P_2$	15.68
$^3D_2$	21.38

Table II. Overlap factors between the configurations [Ar] $2p^{-1}$ 4p and [Ar] $3p^{-2}$ 4p in comparison to overlap factors between [Ar] $2p^{-1}$ and [Ar] $3p^{-2}$.

<nl*|nl>	[Ar] $2p^{-1}$ 4p with [Ar] $3p^{-2}$ 4p	[Ar] $2p^{-1}$ with [Ar] $3p^{-2}$
<1s*|1s>	1.000	1
<2s*|2s>	1.000	1.000
<2p*|2p>	1.000	1.000
<3s*|3s>	0.999	1.000
<3p*|3p>	0.999	1.000
<4p*|4p>	0.895	
P_{if}	0.889	0.993
P_{if}^2	0.790	0.986

Table III. Calculated intensities for the decay channels Ar I* [Ar] $2p^{-1}$ mp - Ar II* [Ar] $3p^{-2}$ np.

	Intensity of final states Ar II* [Ar] $3p^{-2}$ np / %			
Initial state Ar I*	n=4	n=5	n=6	n=7
[Ar] $2p^{-1}$ 4p	79	19	0.2	0.07
[Ar] $2p^{-1}$ 5p	7	38	55	0.6
[Ar] $2p^{-1}$ 6p	2	10	5	74

Table IV. Measured experimental and theoretical shifts in the position of the $L_{2,3}$-$M_{2,3}M_{2,3}$ Auger lines of argon.

Excess Energy E_1 / eV	Experiment $\Delta\varepsilon$ / eV	Error $\delta\Delta\varepsilon$ / eV	Theory[a] $\Delta\varepsilon$ / eV	Theory[b] $\Delta\varepsilon$ / eV
3.3	0.18	0.05	0.24	0.23
5	0.14	0.04	0.2	0.19
7.5	0.08	0.04	0.17	0.16
10	0.03	0.05	0.15	0.14
297.3	-0.07	0.05	0	0

[a]Armen[43].
[b]Van der Straten *et al.*[41].

Table A.I. Calculated values of C_{ave} for a K_α fluorescence L_{23}-$M_{23}M_{23}$ Auger-electron coincidence experiment on atomic argon using a non-magic angle cylindrical mirror analyzer with $\theta = 42.3° \pm 6°$. The incoming x-rays are highly linear polarized with $P = 0.95$ and $\beta = 2$. The fluorescence is detected in z-direction. In the last row values for Cave are listed calculated with Straten *et al.*'s[41] equation for isotropic angular distributions $C_{ave} = 1 - \sqrt{\frac{E_1}{E_A}}$ $E_1 \leq E_A$ and $C_{ave} = 0$ $E_1 \geq E_A$. As seen in the table are the differences minimal and can not be responsible for the discrepancies reported here.

				E_1 / eV					
|i>	|f>	E_A / eV	$\alpha_n \cdot A_2$	2.3	3.3	5	7.5	10	297.3
$^2P_{1/2}$	$^1S_0$	203.1	0	0.893	0.872	0.843	0.807	0.777	-0.083
	$^1D_2$	205.5	0	0.894	0.873	0.844	0.808	0.778	-0.084
	$^3P_2$	207.3	0	0.895	0.874	0.844	0.809	0.779	-0.084
	$^3P_1$	207.1	0	0.894	0.874	0.844	0.809	0.779	-0.084
	$^3P_0$	207	0	0.894	0.873	0.842	0.809	0.779	-0.082
$^2P_{3/2}$	$^1S_0$	200.9	-0.5	0.893	0.872	0.843	0.806	0.776	-0.083
	$^1D_2$	203.3	-0.2205	0.893	0.872	0.843	0.807	0.777	-0.083
	$^3P_2$	205.1	0.3975	0.894	0.873	0.843	0.808	0.778	-0.083
	$^3P_1$	204.9	-0.055	0.894	0.873	0.843	0.808	0.778	-0.083
	$^3P_0$	204.9	-0.5	0.894	0.873	0.843	0.808	0.778	-0.083
		200.9		0.893	0.872	0.842	0.807	0.777	0.000

Figures and figure captions.

FIG. 1. Argon $L_{2,3}$-MM cascade Auger-spectra recorded using exciting photons A) 32.7 eV below the K-threshold; B) 4.9 eV above threshold; and C) on the 1s - 4p resonance.

FIG. 2. Argon energy level scheme derived from the differences in configuration average energies. Two decay pathways of the 1s vacancy are indicated by arrows: The most probable decay via K-$L_{2,3}L_{2,3}$ Auger-process and two subsequent $L_{2,3}$-MM processes, and the process investigated here: the decay through Kα fluorescence followed by $L_{2,3}$-MM Auger-emissions.

FIG. 3. Low resolution argon L23-MM Auger-electron spectra recorded 30 eV below the 1s - 4p resonance (A), 10 eV above the K-ionization threshold (B), and on the 1s - 4p resonance (C). The solid curves in panels B and C are the electron spectra measured in coincidence with K-L_{23} x-ray fluorescence and the dashed curves are the non-coincident spectra.

FIG. 4. Argon $L_{2,3}$-MM cascade Auger-spectra and electron/x-ray coincidence spectra. A) "Normal" L-MM spectrum (photon energy 30 eV below the 1s - 4p resonance). B) Electron spectrum (dashed line) and remaining coincidence spectrum (solid line) at a photon energy 10 eV above the K threshold. C) Electron spectrum (dashed line) and coincidence spectrum (solid line) on the 1s - 4p resonance energy.

FIG. 5. The Auger electron/x-ray fluorescence coincidence spectrum, measured 10 eV above K threshold is represented by the open circles. The vertical marks on the baseline illustrate the calculated L_{23}-$M_{23}M_{23}$ Auger transitions. The bars on top of the spectrum assign the calculated transitions. The calculated transition energies were shifted by -0.7 eV to align better with experiment. The dashed line represents the calculated spectrum in which the finite lifetime of the 2p hole (Γ_{2p}=0.13 eV) and the bandwidth of the CMA (Γ_{CMA}=0.5 eV) were taken into account.

FIG. 6. The Auger electron/x-ray coincidence spectrum measured on the 1s - 4p resonance is represented by the open circles. The vertical marks on the baseline show the calculated spectator transitions from [Ar] $2p^{-1}$ 4p into [Ar] $3p^{-2}$ 4p (also indicated by the upper set of bars on top of the spectra) and the shake-up transitions from [Ar] $2p^{-1}$ 4p into [Ar] $3p^{-2}$ 5p (indicated by lower set of bars on top of the spectra). The calculated transition energies were shifted by -0.7 eV to align better with experiment. The long dashed line represents the total calculated spectrum (spectator and shake-up transitions) in which the finite lifetime of the 2p hole (Γ_{2p}=0.13 eV) and the bandwidth of the CMA (Γ_{CMA}=0.5 eV) were taken into account. The short dashed spectrum is the shake-up part of the calculated spectrum.

FIG. 7. Experimental and calculated PCI shifts of the $L_{2,3}$-$M_{2,3}M_{2,3}$ Auger-transitions in atomic argon. Our experimental values from the coincidence experiment are given by the filled circles (●). The experimental values of Hanashiro *et al.*[46] are given by the filled squares (■) and those of de Gouw *et al.*[47] for the L_2-$M_{23}M_{23}$ (◆) and L_3-$M_{23}M_{23}$ (▲) by the

filled diamonds and triangles. The theoretical values include the influence of experimental broadening and were calculated using van der Straten *et al.*'s[41] (○, open circles) and Armen's[43] (□, open squares) approaches, with E_A = 201.1 eV, $\Gamma_{Lorentz}$ = 0.109 eV and Γ_{Gauss} = 0.5 eV to model the coincidence experiment. The open triangles represent a calculation with E_A = 201.1 eV, $\Gamma_{Lorentz}$ = 0.12 eV and Γ_{Gauss} = 0.1 eV to model de Gouw's results (△, van Straten; ▽, Armen).

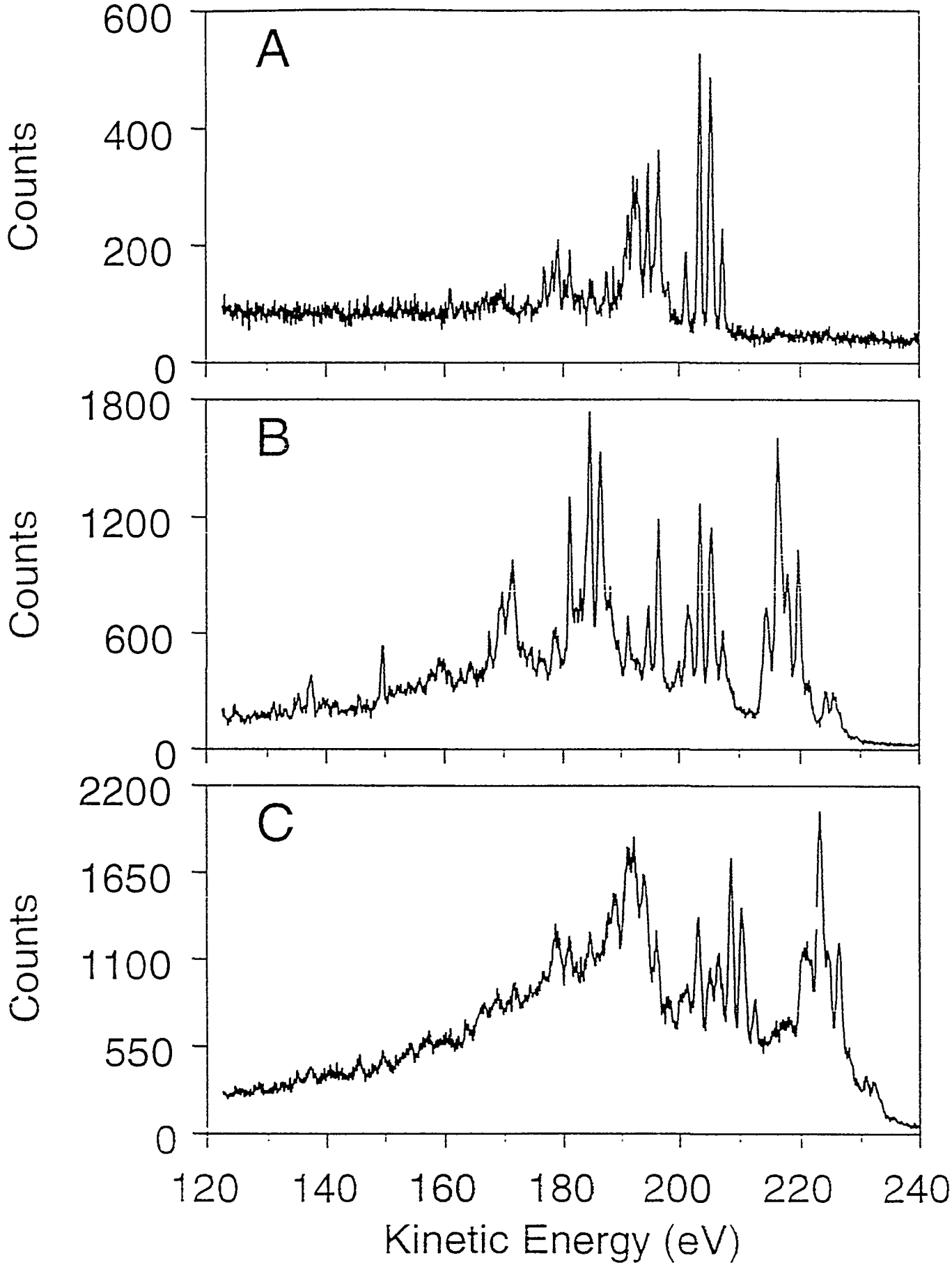
A
B
C
Counts
Counts
Counts
600
400
200
0
1800
1200
600
0
2200
1650
1100
550
0
120
140
160
180
200
220
240
Kinetic Energy (eV)

Fig. -